Investigation of an end-to-end neural architecture for image-based source term estimation

Investigation of an end-to-end neural architecture for image-based source term estimation

A. Abdulaziz, Y. Altmann, S. McLaughlin
School of Engineering and Physical Sciences
Heriot-Watt University
Edinburgh, United Kingdom
a.abdulaziz@hw.ac.uk

M. E. Davies
School of Engineering
University of Edinburgh
Edinburgh, United Kingdom

***Abstract*—Rapid and accurate estimation of hazardous material release parameters, including source location, release time, and quantity of material released, is crucial for protecting assets and facilitating timely and effective emergency response. In this paper, we present a first artificial neural network (ANN) approach for end-to-end source term estimation (STE) using time-series of multispectral satellite images. The architecture consists of two successive ANNs. The first-stage ANN estimates the hazardous material release rate over time, producing a 3D concentration map, while the second-stage ANN utilizes the generated concentration map to estimate the 2D source location, release time, and easterly and northerly wind speeds. By leveraging the inherent nonlinearity of ANNs and advances in parallel computing, our proposed method aims to eventually overcome the limitations of existing optimization and Bayesian inference techniques in handling the nonlinear STE problem. In this preliminary study, we validate the performance of our approach on a simulated dataset, demonstrating its potential for enhancing the accuracy and speed of STE in real-world applications.**

***Index Terms*—source term estimation, artificial neural networks**

I. Introduction

The increasing threat of hazardous material releases resulting from accidents, terrorism [1], or natural disasters, such as the Bhopal gas leak accident [2], the Fukushima nuclear accident [3], and the Eyjafjallajökull volcanic eruption [4], highlights the crucial need for quick and precise estimation of the emission source location, time of release, and quantity of material released. This information is vital to protect public health and enable effective emergency response. Atmospheric dispersion simulation (ADS) models are usually employed to predict the spread of contaminants, assisting in efficient response and post-emergency assessment. Researchers have developed numerous ADS modeling methods, with the Gaussian model being a typical and efficient tool for atmospheric dispersion prediction due to its simple expression [5]. The Gaussian dispersion models (such as the Gaussian puff model and the Gaussian plume model) are particularly suitable for emergency management because of their simplicity and efficiency [6]. Accurate forecasting requires several input variables for the model, including meteorological data, release strength, and location. While meteorological data are generally available from local weather stations or global sources, the strength, location, and release timing often remain unknown and must be inferred from relevant sensor measurements. The development of methods to address this challenge is referred to as inverse dispersion modeling or source term estimation (STE). Incorporating meteorological variables as parameters can account for spatial variations in meteorological conditions, leading to a more accurate overall source estimation. Most STE problems consider individual sensors on the ground or sparse sensor networks. This requires the deployment of assets in the region of interest which may not be possible in remote locations. In this paper, we adopt alternative approach where STE is solved using multi/hyperspectral satellite images which are becoming increasingly available. This, however, assumes that the source of interest is observable using an imaging modality.

STE presents computational challenges due to the intrinsically nonlinear nature of radionuclide diffusion processes in the atmosphere [7]. Two primary approaches are employed to tackle this problem: optimization methods [8]–[15] and probabilistic techniques based on Bayesian inference [16]–[23]. Regardless of the approach, the inferred source parameters are input into a forward ADS model to generate predicted concentrations, which are then compared to observed data using a data fidelity term or likelihood function. The primary objective of these methods is to identify the optimal or most probable match between the predicted and observed data [24]. Both sets of approaches have demonstrated promising results in simulations; however, it has been found that there is substantial potential for improvement when applied to experimental data [24], [25]. Bayesian methods offer the advantage of generating a final estimate with confidence levels and incorporating prior information into the algorithm via probability distributions. This allows for the potential accounting of inaccuracies due to modeling errors or sensor noise, although perfect characterization of these distributions may be challenging, especially in real-world scenarios. On the other hand, optimization methods yield a single point estimate for the source parameters but do not provide confidence intervals for prior information or the final estimate. Despite this drawback, optimization methods are typically less com-

This work was supported by the UK MOD University Defence Research Collaboration (UDRC) in Signal Processing.

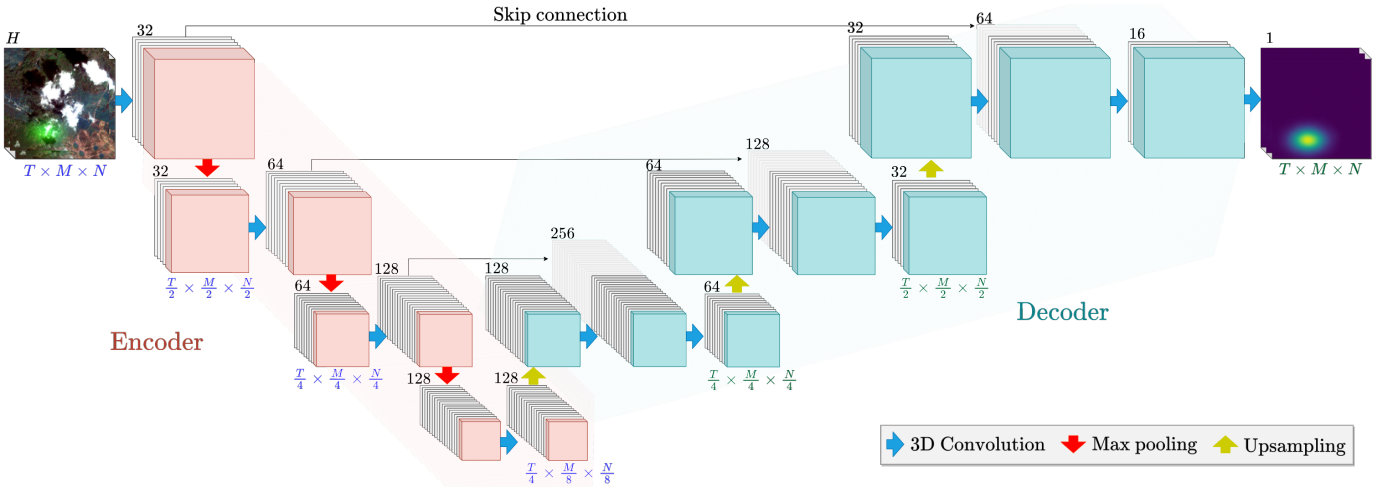

Fig. 1: Schematic of the first-stage of the proposed ANN pipeline
. Arrows of different colors indicate various types of neural network layers, as explained by the color-coding in the legend above.

putationally demanding and may converge more rapidly than Bayesian techniques. Furthermore, they benefit from requiring little or no prior information, although the availability of such information could lead to improved performance.

In recent years, artificial neural networks (ANNs) have emerged as a promising approach to enhance STE [6], [7], [26]–[30]. ANNs can capture complex, nonlinear relationships between inputs and outputs, making them suitable for tackling the inherent nonlinearities of the STE problem. Additionally, deep learning methods can benefit from large amounts of training data, which can lead to more accurate and robust models. Furthermore, advances in parallel computing and hardware accelerators, such as GPUs, have enabled ANNs to achieve faster convergence and real-time performance, making them an attractive option for STE in critical applications. However, existing ANN-based approaches for STE are designed to estimate a subset of the source term parameters such as the release rate [6], [7], [27], [28], [30], the release rate and release time [26], or the source 2D coordinates [29], while the other parameters are assumed known.

In this paper, we introduce a two-stage ANN pipeline designed for estimating source term parameters from time-series hyperspectral satellite images. The first stage of the pipeline focuses on calculating the hazardous material release rate over time, subsequently generating a 3D concentration map derived from the time-series hyperspectral satellite images. The second stage utilizes the 3D concentration map to estimate the 2D source location, the release time, along with the easterly and northerly wind speeds. The effectiveness of the proposed approach is thoroughly validated using a simulated dataset. It is important to highlight that in this study, we assume an instantaneous 2D release simulated utilizing the Gaussian puff model, which is adapted from [14].

The remainder of this paper is organized as follows. In Section II, we introduce the two-stage ANN pipeline adopted in this work for solving the STE problem. The experimental setup and results are discussed in Section III, and finally, we conclude with the key findings and future directions in Section IV.

II. Methodology

Unlike conventional Bayesian and optimization algorithms commonly employed in STE, ANNs offer several significant benefits that make them a more attractive solution for rapid response scenarios. One key advantage is their ability to learn highly non-linear dispersion models directly from training data, eliminating the need for an analytical expression of the forward model, i.e., the cloud formation/evolution model. Moreover, a well-trained ANN can compute predictions in a fraction of a second, providing high computational efficiency that is crucial in time-sensitive situations.

Our objective in this preliminary study is to accurately estimate the following source parameters using ANNs: release rate, 2D spatial source location, release time, and both easterly and northerly wind speeds. The direct prediction of these parameters from hyperspectral satellite images poses a considerable challenge, given the images encompass a diverse range of geographical areas. To address this, we adopt a two-stage strategy. In the first stage, we extract the release rates of hazardous materials from time-series hyperspectral satellite images, generating a 3D concentration map. Subsequently, in the second stage, we utilize the concentration map to estimate the source location, release time, and the two wind speed components. This novel method demonstrates the potential of ANNs to enhance STE in emergency situations, ultimately aiding in more efficient response and mitigation efforts.

A. Two-stage ANN pipeline

The first-stage ANN takes as input a time-series of hyperspectral satellite images with dimensions $T \times M \times N \times H$, containing hazardous material dispersion. Here, T denotes

the temporal dimension, M and N represent the two spatial dimensions, and H corresponds to the channel dimension (i.e, $H = 3$ for RGB but H can be larger for multi/hyperspectral images). The output is a 3D cloud with dimensions $T \times M \times N$, which conveys the spatial concentration of hazardous material over time. As illustrated in Fig. 1, the architecture of the first-stage ANN follows a 3D U-Net design, comprising an encoder and a decoder with skip connections [31], [32]. The encoder consists of four 3D convolutional layers, with the number of feature channels set at 32, 64, 128, and 128 for each layer, respectively. The first three convolutional layers are followed by a 3D max-pooling operation for down-sampling, with pool sizes of $(2\times2\times2)$ after the first two layers and $(1\times2\times2)$ after the third layer. The decoder features three levels. Each level begins with 3D up-sampling of the feature map, using a size of $(1\times2\times2)$ for the first step and $(2\times2\times2)$ for the remaining two steps. Every up-sampling operation is succeeded by a 3D convolution, with the number of feature channels set to 128, 64, and 32, respectively. To enable localization, the output of each convolution is concatenated with the corresponding feature map from the encoder (skip connection). A subsequent 3D convolutional layer is then employed to learn to assemble a more precise output based on the concatenated features, with the number of feature channels set to 64, 32, and 16, respectively. All convolutional layers utilize a kernel size of $(3 \times 3 \times 3)$ and a rectified linear unit (ReLU) activation function. Finally, a $(1 \times 1 \times 1)$ convolution maps each 16-component feature vector to the desired concentration rate. It is important to note that the first-stage ANN can be modified to accommodate more complex observational phenomena, such as changes in illumination or registration errors. Ultimately, it could be integrated as a module into the second-stage ANN.

The second-stage ANN input is the first-stage output, specifically, the 3D extracted cloud with dimensions $T \times M \times N$.

The output of this stage consists of the source term parameters, including release time, the 2D spatial position of the source, and the easterly and northerly wind speeds. As depicted in Fig. 2, the architecture of the second-stage ANN commences with an encoder that shares the same design as the encoder in the first-stage. After the encoder, the two spatial dimensions and the channel dimension are flattened into a single feature dimension, while maintaining the temporal dimension. A Long Short-Term Memory (LSTM) layer containing 2048 units is employed to capture global temporal information. Subsequently, three additional LSTM layers, each consisting of 64 units, are utilized to capture the release time information, source coordinates information, and wind speed information, respectively. The number of LSTM units have been obtained through cross-validation. Finally, three dense layers are used to predict the release time, the 2D spatial coordinates of the release source, and the 2D components of the wind speed.

It is worth noting that the proposed architecture is highly adaptable and can accommodate time-series hyperspectral satellite images of any dimensions $T \times M \times N \times H$. This flexibility allows the model to process a wide range of input sizes, making it suitable for various applications and scenarios.

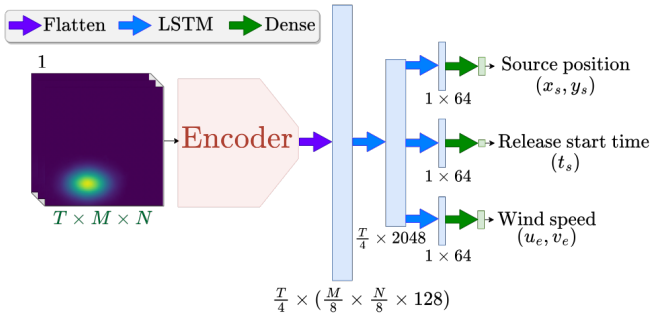

Fig. 2: Schematic of the second-stage of the proposed ANN pipeline. Arrows of different colors indicate various types of neural network layers, as explained by the color-coding in the legend above. The encoder has the same architecture as the encoder of the first-stage with output size $(\frac{T}{4} \times \frac{M}{8} \times \frac{N}{8} \times 128)$.

B. *Two-stage ANN training*

The two stages of the proposed ANN pipeline were trained sequentially, with the second-stage ANN utilizing the extracted 3D concentration map generated by the first-stage ANN. More precisely, we first trained the first-stage ANN and then the second-stage ANN by considering the full pipeline and freezing the first-stage ANN. Both ANNs were trained for 100 epochs using the Adam optimizer [33], with a learning rate of 10^{-3} and a batch size of 30.

The loss function employed for this process is the mean squared error (MSE) loss. In the first branch, the MSE loss is calculated between the true concentration cloud and the predicted cloud, while in the second branch, the MSE loss is determined between the true source term parameters and the predicted parameters. This approach ensures the optimization of both branches for accurate and effective source term estimation.

III. Simulations and Results

An essential aspect of the proposed ANN approach is data preparation, which involves the creation of training and testing datasets. We utilize 320 RGB satellite images with dimensions $968 \times 937 \times 3$ and a 4 m resolution from the Pleiades ESA archive [34]. It is worth noting that in this study we use $H = 3$ (RGB images) for the proof of principle and computational concerns. However, H can be larger for multi/hyperspectral images. To augment the dataset size, we randomly crop 10 sections of size $128\times128\times3$ from each high-resolution image, resulting in a total of 3200 satellite images. Of these, 3000 images are designated for training, while the remaining 200 are allocated for testing.

To simulate instantaneous 2D release of hazardous material over time, we employ the 2D Gaussian puff model, which is adapted from [14] and takes the following form:

$$c(x,y,t) = \frac{q_s}{4\pi\sqrt{\sigma_x\sigma_y}} \exp\left[-\frac{0.25}{(t-t_s)}\times \left(\frac{(x-x_s-u_e(t-ts))^2}{\sigma_x} + \frac{(y-y_s-v_e(t-ts))^2}{\sigma_y}\right)\right], \quad (1)$$

where q_s is the source mass in kg, t_s is the release time, x_s and y_s are the spatial coordinates of the source, u_e and v_e are the easterly and northerly wind speed components, and σ_x and σ_y are the dispersion coefficients. In this context, x and y correspond to a 2D grid with a range of [-63, 64] pixels, covering a range of 512×512 m^2. We set the dispersion coefficients to $\sigma_x = 9$ and $\sigma_y = 4$, which control the dispersion profile. The time t is an integer number in the range [1, T] frames. Here, we assume $T = 20$ frames and the time between two successive frames is 2 sec.

For each of the 3200 RGB images, we generate a random concentration map over time following (1). We randomly select the emission source coordinates, x_s and y_s, within the [-50, 50] pixel range, ensuring the source remains within the field of view. The release time, t_s, is randomly chosen within the [1, 20] frame range. The easterly and northerly wind components, u_e and v_e, are randomly determined within the [-2, 2] pixel range, corresponding to 0 mps, 2 mps, or 4 mps wind speeds. To add the concentration map to the normalised [0, 1] range RGB image, we simulate a mostly green RGB spectrum for the source (Fig. 3), using the same spectrum across the dataset, and set the source mass q_s to 50 kg for a peak source intensity of 0.66 in the green channel. We assume static images over time. Following this, we simulate 3200 cubes of hazardous material dispersion, each with $20 \times 128 \times 128 \times 3$ dimensions, where $T = 20, M = N = 128$, and $H = 3$.

Recall that the first-stage ANN processes a time-series of RGB satellite images containing hazardous material dispersion and generates a 3D cloud representing the spatial concentration of the hazardous material over time. To assess the performance of the first-stage ANN, we present three time frames of one of the testing emission scenarios in Fig. 3. For this particular scenario, the release time, t_s, is frame 3. As shown in Fig. 3 (top row), the concentration map is empty at frame $t = 1$ since there is no emission. At frame $t = t_s = 3$, the ANN successfully extracts the concentration map from the RBG satellite image. Moreover, the model effectively captures the concentration map's evolution over time, as depicted in Fig. 3 (bottom row). Notably, the model can differentiate between the hazardous material release and clouds in the sky, suggesting that the proposed approach is robust under adverse weather conditions. The average MSE between the predicted and true clouds over the 200 testing emission scenarios is 1×10^{-6}, which demonstrates the high fidelity of the ANN approach.

To assess the performance of the second-stage ANN, which processes the extracted 3D concentration map and generates the source term parameters, we present the average MSE between the estimated source parameters and the true values over the testing dataset of 200 emission scenarios in Table I. The results demonstrate that the release time is predicted effectively, with an average MSE of 0.09 frames, indicating the model's efficiency for emergency response applications. Additionally, the 2D spatial coordinates of the emission source are predicted with high accuracy, as evidenced by an average MSE of approximately 1 pixel. Lastly, the easterly and northerly wind speed components are also estimated with high precision, with the average MSE being less than half a pixel. These results underscore the effectiveness and reliability of the second-stage ANN in determining the source term parameters.

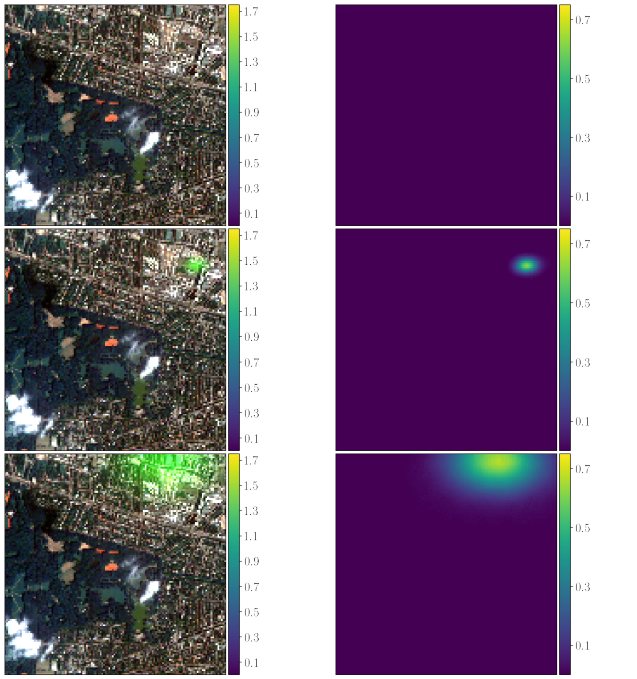

Fig. 3: Estimated concentration maps over time (right panels) obtained from the corresponding RGB satellite images (left panels) using the first-stage ANN. Displayed from top to bottom are the results for frames 1, 3, and 20, with the release time, t_s, set at frame 3.

TABLE I: Average MSE results between the predicted source term parameters from the second-stage ANN and the true values for the testing dataset of 200 emission scenarios.

source term parameter	MSE
x_s	1.16 ± 2.04 (pixels)
y_s	0.99 ± 1.67 (pixels)
t_s	0.09 ± 0.15 (frames)
u_e	0.4 ± 1.52 (pixels)
v_e	0.42 ± 1.65 (pixels)

IV. Conclusions

In conclusion, this study presents a novel two-stage ANN pipeline for source term estimation (STE) using time-series multispectral satellite images, addressing the inherent non-linearity of the problem. By harnessing the power of ANNs and advances in parallel computing, the proposed approach offers a promising solution for rapid and precise estimation of hazardous material release parameters, which is vital for public health protection and effective emergency response management. We have not conducted a comparison of our proposed method with other STE methods due to the challenge of designing a fair comparison. However, this is an important aspect for future work. To improve our pipeline for real-world applications, several areas require further investigation and improvement. Conducting an uncertainty analysis is a crucial

step to evaluate the pipeline's reliability. The performance can be significantly enhanced by refining the encoder-decoder architecture, possibly by incorporating a Variational Autoencoder (VAE) architecture. It's also important to assess how our pipeline performs with irregularly timed and misregistered images, to improve the detection of faint clouds in the imagery, and to work on more realistic data simulations. Reevaluating the training approach for the artificial neural networks (ANNs) is another area worth considering. Instead of training the two-stage ANNs separately, exploring an end-to-end training approach or merging the two successive ANNs into a single network could be beneficial.

REFERENCES

[1] A. Gunatilaka, B. Ristic, and R. Gailis, "On localisation of a radiological point source," in *2007 Information, Decision and Control*, 2007, pp. 236–241.

[2] D. F. VARMA and S. MULAY, "The bhopal accident and methyl isocyanate toxicity," *Toxicology of organophosphate & carbamate compounds*, pp. 79–88, 2006.

[3] T. J. Yasunari, A. Stohl, R. S. Hayano, J. F. Burkhart, S. Eckhardt, and T. Yasunari, "Cesium-137 deposition and contamination of japanese soils due to the fukushima nuclear accident," *Proceedings of the National Academy of Sciences*, vol. 108, no. 49, pp. 19 530–19 534, 2011.

[4] A. Stohl, A. J. Prata, S. Eckhardt, L. Clarisse, A. Durant, S. Henne, N. I. Kristiansen, A. Minikin, U. Schumann, P. Seibert, K. Stebel, H. E. Thomas, T. Thorsteinsson, K. Tørseth, and B. Weinzierl, "Determination of time- and height-resolved volcanic ash emissions and their use for quantitative ash dispersion modeling: the 2010 eyjafjallajökull eruption," *Atmospheric Chemistry and Physics*, vol. 11, no. 9, pp. 4333–4351, 2011. [Online]. Available: https://acp.copernicus.org/articles/11/4333/2011/

[5] N. S. Holmes and L. Morawska, "A review of dispersion modelling and its application to the dispersion of particles: an overview of different dispersion models available," *Atmospheric environment*, vol. 40, no. 30, pp. 5902–5928, 2006.

[6] S. Qiu, B. Chen, R. Wang, Z. Zhu, Y. Wang, and X. Qiu, "Atmospheric dispersion prediction and source estimation of hazardous gas using artificial neural network, particle swarm optimization and expectation maximization," *Atmospheric environment*, vol. 178, pp. 158–163, 2018.

[7] W. Cui, B. Cao, Q. Fan, J. Fan, and Y. Chen, "Source term inversion of nuclear accident based on deep feedforward neural network," *Annals of Nuclear Energy*, vol. 175, p. 109257, 2022.

[8] S. E. Haupt, G. S. Young, and C. T. Allen, "Validation of a receptor–dispersion model coupled with a genetic algorithm using synthetic data," *Journal of applied meteorology and climatology*, vol. 45, no. 3, pp. 476–490, 2006.

[9] L. C. Thomson, B. Hirst, G. Gibson, S. Gillespie, P. Jonathan, K. D. Skeldon, and M. J. Padgett, "An improved algorithm for locating a gas source using inverse methods," *Atmospheric environment*, vol. 41, no. 6, pp. 1128–1134, 2007.

[10] C. T. Allen, G. S. Young, and S. E. Haupt, "Improving pollutant source characterization by better estimating wind direction with a genetic algorithm," *Atmospheric Environment*, vol. 41, no. 11, pp. 2283–2289, 2007.

[11] X. Zheng and Z. Chen, "Back-calculation of the strength and location of hazardous materials releases using the pattern search method," *Journal of hazardous materials*, vol. 183, no. 1-3, pp. 474–481, 2010.

[12] S. K. Singh and R. Rani, "A least-squares inversion technique for identification of a point release: Application to fusion field trials 2007," *Atmospheric environment*, vol. 92, pp. 104–117, 2014.

[13] Y. Liu, S. Fang, H. Li, J. Qu, and D. Fang, "Source term estimation in nuclear accidents using 4d variational data assimilation for heterologous atmospheric condition," in *International Conference on Nuclear Engineering*, vol. 45936. American Society of Mechanical Engineers, 2014, p. V003T06A021.

[14] P. E. Bieringer, L. M. Rodriguez, F. Vandenberghe, J. G. Hurst, G. Bieberbach Jr, I. Sykes, J. R. Hannan, J. Zaragoza, and R. N. Fry Jr, "Automated source term and wind parameter estimation for atmospheric transport and dispersion applications," *Atmospheric Environment*, vol. 122, pp. 206–219, 2015.

[15] S. Fang, S. Zhuang, X. Li, and H. Li, "Automated release rate inversion and plume bias correction for atmospheric radionuclide leaks: a robust and general remediation to imperfect radionuclide transport modeling," *Science of The Total Environment*, vol. 754, p. 142140, 2021.

[16] P. Robins, V. Rapley, and N. Green, "Realtime sequential inference of static parameters with expensive likelihood calculations," *Journal of the Royal Statistical Society: Series C (Applied Statistics)*, vol. 58, no. 5, pp. 641–662, 2009.

[17] R. Lane, M. Briers, and K. Copsey, "Approximate bayesian computation for source term estimation," *Mathematics in Defence*, vol. 2009, 2009.

[18] E. Yee, "Inverse dispersion for an unknown number of sources: model selection and uncertainty analysis," *International Scholarly Research Notices*, vol. 2012, 2012.

[19] H. Rajaona, F. Septier, P. Armand, Y. Delignon, C. Olry, A. Albergel, and J. Moussafir, "An adaptive bayesian inference algorithm to estimate the parameters of a hazardous atmospheric release," *Atmospheric Environment*, vol. 122, pp. 748–762, 2015.

[20] B. Ristic, A. Gunatilaka, and R. Gailis, "Localisation of a source of hazardous substance dispersion using binary measurements," *Atmospheric Environment*, vol. 142, pp. 114–119, 2016.

[21] D. D. Lucas, M. Simpson, P. Cameron-Smith, and R. L. Baskett, "Bayesian inverse modeling of the atmospheric transport and emissions of a controlled tracer release from a nuclear power plant," *Atmospheric Chemistry and Physics*, vol. 17, no. 22, pp. 13 521–13 543, 2017.

[22] P. B. Westoby, L. Delle Monache, and D. Silk, "18th international conference on harmonisation within atmospheric dispersion modelling for regulatory purposes 9-12 october 2017, bologna, italy," 2017.

[23] M. Hutchinson, C. Liu, and W.-H. Chen, "Source term estimation of a hazardous airborne release using an unmanned aerial vehicle," *Journal of Field Robotics*, vol. 36, no. 4, pp. 797–817, 2019.

[24] M. Hutchinson, H. Oh, and W.-H. Chen, "A review of source term estimation methods for atmospheric dispersion events using static or mobile sensors," *Information Fusion*, vol. 36, pp. 130–148, 2017.

[25] N. Platt and D. DeRiggi, "Comparative investigation of source term estimation algorithms using fusion field trial 2007 data: linear regression analysis," *International Journal of Environment and Pollution*, vol. 48, no. 1-4, pp. 13–21, 2012.

[26] B. Wang, B. Chen, and J. Zhao, "The real-time estimation of hazardous gas dispersion by the integration of gas detectors, neural network and gas dispersion models," *Journal of hazardous materials*, vol. 300, pp. 433–442, 2015.

[27] R. Wang, B. Chen, S. Qiu, Z. Zhu, Y. Wang, Y. Wang, and X. Qiu, "Comparison of machine learning models for hazardous gas dispersion prediction in field cases," *International journal of environmental research and public health*, vol. 15, no. 7, p. 1450, 2018.

[28] R. Wang, B. Chen, S. Qiu, L. Ma, Z. Zhu, Y. Wang, and X. Qiu, "Hazardous source estimation using an artificial neural network, particle swarm optimization and a simulated annealing algorithm," *Atmosphere*, vol. 9, no. 4, p. 119, 2018.

[29] A. Fanfarillo, "Quantifying uncertainty in source term estimation with tensorflow probability," in *2019 IEEE/ACM HPC for Urgent Decision Making (UrgentHPC)*. IEEE, 2019, pp. 1–6.

[30] Y. Ling, Q. Yue, C. Chai, Q. Shan, D. Hei, and W. Jia, "Nuclear accident source term estimation using kernel principal component analysis, particle swarm optimization, and backpropagation neural networks," *Annals of Nuclear Energy*, vol. 136, p. 107031, 2020.

[31] O. Ronneberger, P. Fischer, and T. Brox, "U-net: Convolutional networks for biomedical image segmentation," in *Medical Image Computing and Computer-Assisted Intervention–MICCAI 2015: 18th International Conference, Munich, Germany, October 5-9, 2015, Proceedings, Part III 18*. Springer, 2015, pp. 234–241.

[32] Ö. Çiçek, A. Abdulkadir, S. S. Lienkamp, T. Brox, and O. Ronneberger, "3d u-net: learning dense volumetric segmentation from sparse annotation," in *Medical Image Computing and Computer-Assisted Intervention–MICCAI 2016: 19th International Conference, Athens, Greece, October 17-21, 2016, Proceedings, Part II 19*. Springer, 2016, pp. 424–432.

[33] D. P. Kingma and J. L. Ba, "Adam: A method for stochastic gradient descent," in *ICLR*, 2015, pp. 1–15.

[34] E. S. Agency, "Pleiades." [Online]. Available: https://earth.esa.int/eogateway/missions/pleiades